Synthesis, Characterisation and Cytotoxicity of Gold Nanowires for Ultra-Sensitive Biosensor Development

Nurul Akmal Che Lah
Universiti Malaysia Pahang Fakulti Kejuruteraan Pembuatan https://orcid.org/0000-0001-8530-1061
Robert Gray
University College London Medical School
Sonia Trigueros (sonia.trigueros@zoo.ox.ac.uk)
University of Oxford https://orcid.org/0000-0001-5621-7303

Research

Keywords: nanobiosensor, biomarkers, antimicrobial, cytotoxicity, gold nanowires

Posted Date: October 27th, 2020

DOI: https://doi.org/10.21203/rs.3.rs-49469/v3

Version of Record: A version of this preprint was published on February 17th, 2021. See the published version at https://doi.org/10.1186/s12934-020-01478-y.

Abstract

With the long-term goal of developing an ultra-sensitive microcantilever-based nano biosensor for versatile biomarker detection, new controlled bioreceptor-analytes systems are being explored to overcome the disadvantages of conventional ones. Gold nanowires (AuNWs) have been used as a probe to overcome the tolerance problem that occurs in response to changes in environmental conditions. However, the cytotoxicity of AuNWs is still unclear. Here, we examined the cytotoxicity of AuNWs systems using both commercial and as-synthesised AuNWs. *In vitro* experiments show that commercial AuNWs with an average quoted length of 6 μm are highly toxic against Gram-negative *Escherichia coli* (*E. coli*) at 50 μg/ml. However, this toxicity is due to the presence of CTAB surfactant not by the nanostructure. Conversely, the as-synthesised AuNWs with an average length of 9.5 μm show non-cytotoxicity even at the maximum viable concentration (330μg/ml). These findings may lead to the development of potentially life-saving cytotoxicity -free nano biosensors for an early diagnostic of potential diseases.

1. Introduction

A wide array of biomarkers secreted by cancerous cells can be found in blood samples [1-6]. With current emerging proteomics technologies, it is straightforward to obtain reliable sets of disease-specific protein biomarkers. Early identification of disease blood protein signatures, is becoming the most promising strategy for effective cancer prevention [7-10]. Nevertheless, some protein biomarkers, such as those secreted by cell death in tumours microenvironment at a very early growth period, are produced only at ultra-low concentrations [11-14]. Low reproducibility highlights the difficulty in detecting low concentrations of disease protein biomarkers. With concentration, the scales are six to seven orders of magnitude lower than the plasma protein (e.g. the reference range of albumin protein in blood is approximately 35-55 g/L [15, 16]), making their detection challenging. Engineered nanomaterials-based biosensors with high sensitivity levels have been the focus of improved biomarker detection technology [17-21]. These advanced detection methods depend on the antibody and protein for recognition, identification and quantification of targeted cells.

There are several drawbacks on microcantilever (MC) biosensor, MC requires a high amount of analytes and should be sensitive enough to measure deflection in the range of few nanometres leads [22-24] to the integration of microfluid nano-biosensor layer for protein-protein interaction detection [25]. Hence, nanomaterial-based MC biosensors have good potential in advanced biosensor technology as they offer a high surface-to-volume ratio, so they are able to mediate faster with a higher kinetic electron transfer, allowing the merit of multiple sensing mechanisms in a single platform [26-29]. The size of nanomaterials can facilitate effective interaction depending on the nature of the chemical bonding with targeted biomolecules in opaque liquids such as blood or urine [30-34]. Furthermore, since the dimension of nanomaterials is comparable to the Debye length, their specific surface properties affect the kinetics and electron transfer significantly [35-37]. Offering potential for electronic detection surface stress functionalisation as a result of the MC bending by a certain extent generated by analyte-ligand interactions in the biomarker layer.

Gold (Au) based one-dimensional (1-D) nanomaterial is a candidate for achieving an ultrasensitive MC biosensor device [38-43]. Specifically, for flexible chemo resistive sensors.Au nanowires (AuNWs) are attractive because they possess minimal cross-sectional area but have the ability to increase the flood-current along the axial current direction, resulting in higher conductance changes compared to the typical zero-dimensional (0-D) nanomaterials [44, 45]. The chemoreceptive characteristics of AuNWs such as the capability to serve as biocompatible surface for the immobilisation of biomolecules in a correct orientation which enhances the binding affinity of antigen-antibody and the ability to support a swift electron-transfer which causes the flow of one-way electron between two electrodes are key considerations in designing the MC nano biosensor [46-51]. Chemoreceptive and also conductometric characteristics played by the AuNWs are both important for biosensor transduction mechanism.

On the other hand, there have been many concerns about the potential cytotoxicity of nanomaterials in general, which may arise upon medical application [52-55]. It has been proved that several quantum materials consisting of heavy metals may release ions that may cause cytotoxic effects. Although AuNWs are not considered toxic in most cases, there is a certain ambiguity about AuNWs toxicity impact regarding variability and threshold for specific cell types [56-58]. Therefore, there is an urgent need to present new data that can assist in developing a mass-sensitive MC-based AuNWs biosensor. Important primary parameters that are involved in cytotoxicity assessments of AuNWs include the aspect ratio of nanowires, surface functionalisation method, cell type, administration of dosage and application protocols. In this work, we describe the synthesis of bio-friendly AuNWs for MC biosensor application. The objective is to ascertain the maximum dose of as–synthesised AuNWs, which is safe to avoid initial cytotoxicity whilst increasing the sensitivity of the nanowires array in comparison with commercial AuNWs suspended in CTAB. Bacteria cells are the most sensitive cells to detect toxicity arising from either free or nanostructured metallic ions. For toxicity detection, we use a set of antimicrobial approaches. The transduction mechanism of nanosensors depends on the binding of the protein of interest change which yields different conductivity output. The AuNWs play a vital role in the transduction mechanism. Hence it is essential to maximise the concentration of AuNWs to achieve maximum sensitivity. The investigation of the transduction mechanism is not within the scope of this study. The assembling nanowires on the top surface of the microscopy probe is also evaluated but not discuss further in the present study and only included in the Supplementary Materials section. Any biomarker should be able to be detected using this platform.

2. Materials And Methods

2.1 Ultra-thin AuNWs Preparation

Oleylamine, OA (technical grade 70%), triisopropylsilane, TIPS (98%), hexane ($CH_3(CH_2)_4CH_3$, anhydrous, 95%) and ethanol (CH_3CH_2OH, absolute, ≥99.8%) were purchased from Merck Sigma-Aldrich, United Kingdom. All the chemicals were used without further purification.

Commercial AuNWs (dispersion in H_2O, contains cetyl trimethyl ammonium bromide, CTAB as a stabiliser) used was purchased from Merck Sigma-Aldrich, United Kingdom. The AuNWs is specified to have an average diameter size and length of 30 nm and 4.5 m, respectively, with a concentration of 50 g/mL.

2.2 Microbial Cell Culture Preparation

The commercial *Escherichia Coli (E.coli) DH5-Alpha strain (DH5α),* an engineered non-pathogenic strain for routine subcloning procedures is used in the present work. It is quick and easy to grow and has been used extensively as a lab microbial model system. (ThermoFisher catalogue number 18263618). *E.coli* cells were grown in Luria-Bertani medium (LB), rich medium for cell growth. The cells were initially grown from an original culture sample, kept at -80°C. Cells were inoculated onto an LB agar plate and incubated at 37°C for 24 hours. At this point, a number of individual colonies had grown, each from a single cell. To reduce variation across the bacteria under study, a single colony was selected and incubated in LB to produce a working cell solution. This was used as the master cell culture for all the bacteria cell experiments. Optical cell density measurements were acquired using a Perkin Elmer Lambda Bio$^+$ Spectrophotometer (Germany). The spectrophotometric method measured the optical density at 600 nm based on an American Public Health Association (APHA) standard. The optical density (OD) of 0 is set for pure LB, and the spectrophotometer is calibrated so that the OD equal to 1.00 corresponds to a cell density of 109 ± 5 x108/ml. A linear relationship between OD and cell density is achieved over this range.

2.3 Cytotoxicity Validation Methods

2.3.1 Disk Diffusion Assay

Cytotoxicity test is carried out through the agar disk diffusion assay method which has been used in many clinical microbiology laboratories for routine antimicrobial susceptibility testing. The standard measurement is based on the Clinical Laboratory Standard Institute (CLSI) and manufacturers' standard for each sample. The AuNWs colloidal solution (300 µg/ml) was suspended in distilled water and this portion deposited on the sterile paper disk that is 6 mm in diameter with 4 replicate disk per sample. The disk was placed on Gram-negative *E. coli DH5α* strain. Controls were prepared using pure hexane and/or distilled water.

E.coli DH5α were inoculated at a concentration of 107 to 108 cells/ml at stationary phase strain onto Luria-Bertani (LB) agar. The LB agar plates were then inoculated and incubated for 24 hours at 37°C to record the cytotoxicity effect. The size of the inhibition zone around the disc is control by the interchange between the AuNWs diffusion rate (Eq. 1), the exponential growth rate of the bacteria and the minimum inhibitory concentration which is usually higher than the breakpoint.

$$C(r,t) = \frac{A.e^{\left(\frac{-r^2}{4Dt}\right)}}{4\pi hDt} \qquad (1)$$

The *C* is referring to the AuNWs concentration at time (*t)* and distance (*r)* from the point source (disc centre) with the diffusively isotropic assumption in a 2-D plate form. The *D* is the corresponding diffusion coefficient and *A* is the amount of initial AuNWs used in the disc with *h* is the height of the agar in the plate. The concentration of AuNWs in the inhibition zone could drop below the minimum inhibitory concentration after overnight incubation. By this time, the diffusion of the nutrient in the plate occurs and gradually depleted by the bacteria that grew in the inhibition zone periphery. Overnight incubation made the cells cover almost 70% of the growing surface, except for the circles of growth surrounding disc which remained clear. The diameters of these circles are then measured and used as measurements of the inhibitory effects of the sample.

2.3.2 Colony Forming Unit Counting Method (CFU)

Methods for *in vitro* evaluation of antimicrobial activity, seek to assess the total number of *E.Coli* cells in culture media [59]. Colony-forming units (CFU) of *E. coli DH5α* were counted after plating triplicate serial dilutions of LB cultures on LB-Agar plates and incubating overnight at 37°C. Plates containing between 2 and 200 individually identifiable colonies were counted. The relative number of colonies on a plate compared to the control gives a value which is a measurement of the toxicity.

2.4 Nanostructures Characterisation Methods

2.4.1 Characterisation of As-Synthesised and Commercial AuNWs

AuNWs were resuspended and sonicated in ethanol medium. And let it dry on an aluminium substrate at room temperature. Field emission scanning electron microscopy (FESEM) imaging was conducted by a JEOL JSM 7500 F microscope equipped with a cold field emission gun at an acceleration voltage of 15 kV. An in-lens detector collected secondary electrons and backscattered electrons signals and in-chamber multi-quadrant annular retractable solid-state detector, respectively. Element analysis was carried out using Zeiss Neon 40EsB (Carl Zeiss NTS GmbH, Oberkochen, Germany) at 20kV equipped with energy dispersive x-ray spectroscopy, EDX (Inca software, Oxford Instruments). Image analysis on FESEM data was carried out using ImageJ 1.50i. AuNWs density was determined using the plugin ‘analyse particles’ function of ImageJ on a total of 20 SEM images of AuNWs samples. The aggregated size of AuNWs was calculated from a total of 2000 randomly picked aggregated AuNWs from FESEM images.

3. Results

3.1 Synthesis of Ultra-Thin AuNWs

AuNWs were synthesised based on the method described in the literature [60]. In the absence of heat, the synthesis reaction involved mixing of 100µl OA and 150 µl TIPS with about 3 to 5 mg of gold (III) chloride precursor solution, ($HAuCl_4$ 99.9% trace metals basis, 30 wt.% in dilute HCl) in 2.5 ml final volume of hexane without stirring. OA acts as a stabiliser and a template for 1-D growth with TIPS role as a highly reactive reducing agent. The observation of the reaction through the change in colour from light orange to red, followed by dark violet during the period of reaction left out at room temperature is demonstrated in **Figure 1**. The AuNWs products were centrifuged, washed with ethanol at least 3 times and finally re-dispersed in hexane for further characterisations. Nanowires produced, according to the published method, have diameters of about 2 nm, lengths of a few µm and self-assembled on deposition into organised structures. In this work, the resulting AuNWs were 3 nm in diameter with a standard deviation of 0.8 %. During the synthesis reaction, the potential of Au^+ reduction to Au is higher in the presence of OA [61-64]. The primary limiting factor for constant electron transfer rate would be the OA reagent. The relative concentration of the AuNWs obtained was > 50µg/ml. This method can also be applicable for the synthesis of other metal nanowires as long as the chemical combination is suitable and correct.

3.2 Morphological Properties of Synthesised Ultra-Thin AuNWs and Commercial AuNWs

The as-synthesised AuNWs samples obtained were characterised for their morphological properties by standard techniques. The morphology, distribution and purity of the as-synthesised AuNWs verified by FESEM are shown in **Figure 2A**. For a 24 h reaction, the resultant colloid colour is dark violet which indicates extended filament-like structures. The AuNWs tend to self-assemble into 1-D networks and forming closely packed parallel structures. The use of negatively charged TIPS in the synthetic reaction at room temperature controls the acceleration of the process [65, 66]. The size distribution of parallel AuNWs bundles was difficult to measure. Higher magnification of the assembled ultra-thin AuNWs was unachievable due to their highly sensitive towards the electron beam which resulted in melted nanowires within a few seconds of exposure. However, it is expected that the ultra-thin AuNWs possess diameters of approximately smaller than 3 nm with an aspect ratio (length-to-width ratio) above 1000 nm as the method was re-created from the existing work of [60] and proved in the published figure with the asterisk mark. In this case, the AuNWs tended to form a stack of parallel bundles (yellow rectangular) which then self-assembled into 1-D network structures over macroscopic distances through a spontaneous directional aggregation that occurs during solvent evaporation. The directional aggregation is typically formed *via* oriented attachment in which AuNWs are permitted to fuse as the chemical potential between each chain is different. Therefore, the smoothing extension process to interconnect the nanoparticles of the nanowires takes place through diffusion. The AuNWs exhibit higher stability in a polar solvent which is favourable for the subsequent immobilisation of biomolecules. The ultra-thin self-assembled networks of individual crystalline AuNWs with a gap distance of ~2 nm can be of use to trap the analyte molecules and automatically locate them within the gap of closely packed parallel AuNWs making them as suitable substrate candidates for SERS studies due to the presence of closely packed ‘hotspot’.

The primary objective of this work is to produce ultra-thin AuNWs with high aspect ratio and analyse the elements of samples with the quantitative and qualitative analyses properties. **Figure 2B** shows the

element composition of obtained AuNWs samples using EDX. The EDX point measurements were carried out for an accurate estimation of Au amount present in each sample. For as-synthesised AuNWs, the amount of Au is at the level of 98% as the major element in the sample with the remaining amount is Si (substrate). The presence of high purity Au has resulted from homogeneous nucleation of metallic Au as spherical clusters and hence determined the growth of 1-D nanowires. This condition proves that in the presence of TIPS, Au seeds have rapid kinetics in the formation of nanowires. **Figure 2: A**. The representative FESEM micrograph of the as-synthesised AuNWs. The enlarged figure (yellow rectangular) reveals the parallel self-assembly arrangement of close-packed AuNWs bundles. The small parallel bundle highlighted in yellow circle showed that the bundle of the nanowires has a diameter size of ~200 nm. Noted that the individual AuNWs in each bundle would possess the arrangement and the individual AuNWs size that are almost similar to the original method reported by Feng et al., (*Figure with asterisk mark is reproduced from ref. [60] with permission from The Royal Society of Chemistry*). **B**. The EDX spectrum analysis of the as-synthesised AuNWs recorded for the selected area of AuNWs (red rectangle) taken from image **A**.

On the other hand, the representative FESEM images of commercial AuNWs suspended in CTAB aqueous solution are shown in **Figure 3**. It has been observed that the network formed does not assemble into ordered nanostructures (**Figure 3A**) as seen in the as-synthesised AuNWs sample beforehand. Instead, the commercial AuNWs are randomly self-gating forming junction connection. Some of the AuNWs showed thicker diameter with reduced lengths as demonstrated in **Figures 3B** and **3C**. The AuNWs can be as long as 171 m (**Figure 3D**).

One can see that the diameters of the nanowires were averagely thin and approximately ~540 nm as indicated in **Figure 3E**. Interestingly, the specified by the supplier is ~30 nm. It is common to have different values of diameter and length from the specified information properties provided by the supplier as they are in a discrete condition and slight changes in the physical handling, as well as the time storage, would affect the properties of the sample. The procedure in preparing the FESEM analysis would contribute to the alteration on the morphologies and diameter size of the AuNWs. Apparently, Au, in its nature, is quite malleable [67-70]. Hence, the possibility for the AuNWs to break during sonication bath is higher [71, 72]. Although the ultrasonic bath is used for homogenising the nanowires dispersion without major damage to the nanostructures, the excess energy presence, especially towards malleable nanomaterials would lead to significant particle-particle fusion. Additionally, it is reported that the smaller nanowires with large surface-to-volume ratio would have a high surface recombination rate [73, 74] that further increase the collision frequency. Thus, it facilitates the aggregation, which also correlates to the changes of their stability property. CTAB is used to minimise the aggregation, but it would not be able to halt the entire aggregation of the AuNWs. In this case, CTAB is considered as an effective stabiliser which proved by the average diameter, distribution provided in the histogram (**Figure 3E**). The distribution is dominantly conquered by the 540 nm based on the highest per cent frequency distribution (68%), while the larger nanowires (~1.25 to 7.14 μm) with the per cent frequency is only 3% measured by the Gaussian distribution. This indicates that the 540 nm of majorly contributes to the overall properties of the sample.

The average length of nanowires, typically remained the same caused by the similar diffusion of intense high energy ions in the surrounding. The polydispersity distribution of the commercial AuNWs is shown in **Figure 3F**. The narrow length distribution range (up to ~ 30 m) indicates that the commercial AuNWs were stable and monodispersed. The wide distribution range is due to the more considerable length variation, which is up to ~ 171 m.

It shall be noted that the cloudy region encircling AuNWs is due to the strongly coupled capping action of CTAB upon the evaporation of the solvent, leaving the residue behind. Since cationic CTAB surfactant consists of long carbon atomic chain [75-78], it functions as space-filling of secondary material that fills up the gaps between the AuNWs and maintains the individual distribution of AuNWs. The FESEM micrographs distinctly manifest dissimilarity of CTAB grain with AuNWs, exhibiting large-sized flake grains (marked with the blue arrow in **Figure 3**). As stated in few reports [79-81], the tertiary ammonium ion cationic headgroup in the presence of bromide anion as a counterpart in nanowire solution results in higher binding affinity and leads to more stable bilayer on the nanowire surface. The addition of CTAB micelle helps to stabilise AuNWs when the equilibrium condition is achieved through the occupation some of the surface areas caused by the increased in the aggregation number of CTAB micelle. This stabilisation effect, while making them soluble, can be an inhibitor of subsequent self-assembling process.

3.3 Cytotoxicity Evaluation of As-Synthesised and Commercial AuNWs

The proof-of-concept on the cytotoxicity of the nanosensors-based nanowires requires long acquisition times. Some of the nanowires conventional synthesis protocols, such as the reduction of Au precursor in the presence of capping agent can introduce toxic materials from surface conditioning and chemistry [82, 83]. These including surface charge and capping stabilisation without ‘green’ physical approach profited from natural nanostructure generation [84, 85]. Additionally, the metal itself can produce toxicity and thus, being unfavourable for *in-vivo* applications. Taking into consideration the unique advantages of AuNWs, different capping interface, these types of AuNWs exhibits a significant effect in microbial viability. For this reason, we examined the potential cytotoxicity propensity for commercial and as-synthesised of AuNWs.

To further demonstrated the cytotoxicity tolerance in as-synthesised and commercial AuNWs samples, the commercial bacteria *E.coli DH5α*, an engineered non-pathogenic bacterial strain is extensively used as a lab cytotoxicity microbial model system. Two types of cytotoxicity test were carried out. The first is the disc diffusion assay. This method is performed to detect cytotoxicity by inducing a gradient of concentration (**Figure 4A**) around a disc (known as inhibitory effect) loaded with AuNWs. The inhibitory effect among the *E.coli DH5α* strains exhibited different outcomes. The ratio of the ring area (measure in mm) is directly proportional to the sample toxicity (white lines) as indicated in **Figures 4B and 4C**. The results show that the gradient of commercial AuNWs suspended in CTAB halts the growth of bacteria and creates an inhibition zone around the disc in both the 10 and 50 g/ml samples. Lower inhibition zone was found for 1000 g/ml Au ions. For these types of Au-based suspensions, the largest inhibition zone

reached 3.9 0.2 mm, 2.9 0.3 mm and 1.2 0.1 mm for 50 g/ml commercial AuNWs-CTAB, 10 g/ml commercial AuNWs-CTAB and 1000 g/ml Au ions, respectively. Non-toxic samples with no inhibitory effect which refer to water (**Figure 4D**) and hexane (**Figure 4E**) samples. A similar observation was found for 400 g/ml Au ions and <330 g/ml as-synthesised AuNWs suspended in hexane. The six samples used to observe the average diameter of inhibition zones containing Au-based solutions is presented in **Figure 4F**.

The size of as-synthesised AuNWs prepared with growth solution contained AuNWs with a smaller length. Since hexane is a non-polar solvent, it has no charge. Thus, the conjugated surface of AuNWs with negatively charge of the hydrophobic OA, yield a negative surface charge of the AuNWs system [86, 87]. As a result, no electrostatic interactions due to absent of different charges in the solution between the cell surface and as –synthesised AuNWs suspended in hexane. As generally accepted, CTAB alone is highly

toxic cationic surfactant [88-90] and the conjugate systems of AuNWs-CTAB are proven to still contribute to toxicity to culture cells especially when the elevated concentrations of CTAB are present (50 g/ml commercial AuNWs-CTAB). With increasing the amount of AuNWs-CTAB solution, the cytotoxicity of the sample is increased caused by the nonspecific binding tendency of CTAB to negatively charged cell surfaces by electrostatic interactions [91, 92]. Once the interaction with the cell occurs, it forms blebs and holes on the cell and leading to cell death evident by the increase in the diameter of the ring zone. Moreover, the data also suggest that the abilities to induced cell death are also significant regardless of the aspect ratio of the AuNWs, in this case, the aspect ratio is constant for both 10 and 50 g/ml commercial AuNWs-CTAB solution. To minimise the cytotoxicity effects in AuNWs-CTAB, the interaction between the membrane cell and CTAB should be blocked by using protein types of coating on the bilayer surface of CTAB. Meanwhile, a similar trend of nonspecific binding also observed when Au ions are incubated with the cell. The nonspecific binding was evident by the increased of the ring zone when exposed to the concentration of the 1000 g/ml Au ions. This nonspecific binding did not take place with 400 g/ml Au ions might be due to the reduced content of positively charge Au ions, which in turn, decreases electrostatic interaction between the Au ions and negatively charged cell membrane. These results affirm cytotoxicity potency of commercial AuNWs -CTAB and Au ions compared to as-synthesised AuNWs suspended in hexane.

For further validation of cytotoxicity detection on commercial and as-synthesised AuNWs, the CFU enumeration is carried out after 24 h incubation (**Figure 5A**). As evident from **Figure 5B**, the CFU enumeration for 10 g/ml Au ion measured viability of 72%. At 30 g/ml Au ion approximates value were almost similar to the other one giving rise to 69%. Cell-viability assessed by CFU remained at 100% on the control (water) sample. Compared with 10 and 30 g/ml of Au ions, the cell incubated with a higher concentration of Au ions (100 g/ml) was observed to be 0% cell viability. In the case of 2 g/ml of commercial AuNWs suspended in CTAB, <300 g/ml as-synthesised AuNWs and hexane also, 0% were viable for all in CFU enumeration. Pure hexane, water and the ionic Au at three different concentrations (10, 30 and 100 g/ml) were used as negative controls. Assessment at 96 hours was likely to be optimal for AuNWs strain. Indeed, the effect of both commercial and as-synthesised AuNWs along with a high

dosage of 100 g/ml Au-based ion seemed strong antibacterial agent in this assay. Considering the high amount concentration use for as-synthesised AuNWs, it is suggested that the AuNWs work markedly better, meaning presents less bacteria toxicity than Au ions (tenfold lower in concentration) as happened to other metallic materials.

Endowing the high antibacterial potency or toxicity effect based on the viability results for both types of AuNWs at those particular concentrations, another study is carried out to compare the inhibiting capability of commercial AuNWs-CTAB with AuNWs-sodium bicarbonate ($NaHCO_3$) towards the cell growth. The focused study is purposely done on the commercial AuNWs-CTAB since a relatively low amount of sample concentration used proved to affect the cell viability significantly. To further clarify the inhibitory antibacterial activity induced by the CTAB layer, commercial AuNWs were purified from CTAB capping layer and re-dispersed in 2 mM $NaHCO_3$. Cells grown in LB media with AuNWs-CTAB and AuNWs $NaHCO_3$ with an approximate volume of 250 µl for both were observed. Water served as the standard control. The cell-nanowire-LB solutions were approximately 5µg/ml, incubated for 90 minutes and was serially diluted to 105 times of the initial concentration with the set to dispense for 100 µl onto plates. As shown in **Figure 5C**, CFU enumeration showed 4 % and 130% of capture efficiency for AuNWs-CTAB and AuNWs-$NaHCO_3$ solutions, respectively. The low CFU in the CTAB solution was found to be threefold lower than in $NaHCO_3$, indicating that the toxicological effect of CTAB is relatively high, which significantly displayed susceptible inhibit growth of *E.coli* cells. $NaHCO_3$ had a low inhibitory effect.

The results demonstrated that surface modification is the decisive factor governing the cytotoxicity of AuNWs. CTAB proved the capability to induce *E.coli DH5a* cell death and destroy bacteria growth. As regards to the surface modification, the AuNWs capped with $NaHCO_3$ (well-known as baking soda), indicated minimal toxicity effect and had almost no effect on cell viability in an alkaline environment. The alkaline environment retarded the activity of the toxicity which inhibits the cellular uptake. When combining with $NaHCO_3$, the acidic environment that usually leads to cell death is halts and decreasing the risk of adverse effects and toxicity.

It is believed that the primary toxicity mechanism of the AuNWs-CTAB was via the activation of intracellular cell damage, which rigidly controls the per cent of cell survival. As the cell tries protecting itself from toxicity created by the molecule, other existing plasma proteins will adsorb on the surface of nanowires. The nanowires eventually penetrate the cells after adjusting the interfacial properties of the adsorbed protein shell. However, some of the adjustments are not always a success as not all modified AuNWs surface would able to enter the cells effectively. The proper conjugated AuNWs able to recognise the proteins on the cell membrane. Thus, adsorption of the protein to the surface of the nanowires mediate the direct penetration of nanowires. Typically, smaller AuNWs are frequently deemed as more toxic due to the ability to fully penetrate at intracellular locations (*e.g.*, nucleus) which is not able to get through by larger nanostructures. Hence, since cytotoxicity was controlled by the physicochemical surface properties (surface charge number and dimensions) of AuNWs, it is crucial to employ riskless

surface modification reagent to govern the biological effects of nanowires to ensure the safety of nanostructures used in medical applications.

4. Conclusions

As discussed, the synthesis of AuNWs has tailored ultra-thin nanowires that formed the irregular chain-like oriented assembly. These ultra-thin AuNWs in hexane solution are almost similar in average length and ten times smaller in diameter size as compared to commercial AuNWs suspended in CTAB solution. However, they are unstable at relatively high temperatures, melting within a few seconds upon the heat exposure. The anionic polymer of OA was used as a capping layer to protect as-synthesised AuNWs from aggregation, which also render them to be biocompatible. The feasibility of the AuNWs reveals that the functionalised AuNWs in the present of OA was able to avoid cytotoxicity to the membrane cell. On the other hand, the commercial AuNWs in high crystallinity state are stable at elevated temperatures and the toxicity responds observed is mainly caused by the CTAB capping layer and not due to the aspect ratio of the AuNWs. In fact, the pristine AuNWs alone was generally non-toxic and proved to have low cytotoxicity when capped with $NaHCO_3$ upon eliminating the CTAB layer on the nanowires. These different surface modifications have shown that the cytotoxicity of AuNWs is closely related to the original physicochemical properties of the capping layer based on the *in vitro* cell investigation results. Hence, the as-synthesised AuNws and the AuNWs- $NaHCO_3$ could be considered as the optimal options for integrating and implanting in MC biosensor devices, including high-throughput applications.

Declarations

Author Contributions: ST. conceived and designed the experiments; ST, RG and N.C.L performed the experiments. ST, RG and N.C.L wrote the manuscript**.**

Acknowledgements: All individuals listed as authors have contributed substantially to the experimental and discussion of the reported work. ST and RG were supported by EPSRC IAA D4D00620. S.T. also acknowledges support from the Oxford Martin School and EasternBiotech.UK. N.C.L was supported by University Malaysia Pahang RDU1703152 and RDU190360.

Conflicts of Interest: “The authors declare no conflict of interest.”

References

1. Zaidi, S.A., F. Shahzad, and S. Batool, *Progress in cancer biomarkers monitoring strategies using graphene modified support materials.* Talanta, 2020. **210**: p. 120669.
2. Bermúdez-Humarán, L.G., P. Kharrat, J.-M. Chatel, and P. Langella, *Lactococci and lactobacilli as mucosal delivery vectors for therapeutic proteins and DNA vaccines.* Microbial Cell Factories, 2011. **10**(1): p. S4.

3. Teusink, B., H. Bachmann, and D. Molenaar, *Systems biology of lactic acid bacteria: a critical review.* Microbial Cell Factories, 2011. **10**(1): p. S11.
4. Ruhen, O. and K. Meehan, *Tumor-Derived Extracellular Vesicles as a Novel Source of Protein Biomarkers for Cancer Diagnosis and Monitoring.* Proteomics, 2019. **19**(1-2): p. 1800155.
5. Johnsen, K.B., J.M. Gudbergsson, T.L. Andresen, and J.B. Simonsen, *What is the blood concentration of extracellular vesicles? Implications for the use of extracellular vesicles as blood-borne biomarkers of cancer.* Biochimica et Biophysica Acta (BBA)-Reviews on Cancer, 2019. **1871**(1): p. 109-116.
6. Jalalian, S.H., M. Ramezani, S.A. Jalalian, K. Abnous, and S.M. Taghdisi, *Exosomes, new biomarkers in early cancer detection.* Analytical biochemistry, 2019. **571**: p. 1-13.
7. Pashayan, N., A.C. Antoniou, U. Ivanus, L.J. Esserman, D.F. Easton, D. French, G. Sroczynski, P. Hall, J. Cuzick, and D.G. Evans, *Personalized early detection and prevention of breast cancer: ENVISION consensus statement.* Nature Reviews Clinical Oncology, 2020: p. 1-19.
8. Loktionov, A., *Biomarkers for detecting colorectal cancer non-invasively: DNA, RNA or proteins?* World Journal of Gastrointestinal Oncology, 2020. **12**(2): p. 124.
9. Lima, Z.S., M. Ghadamzadeh, F.T. Arashloo, G. Amjad, M.R. Ebadi, and L. Younesi, *Recent advances of therapeutic targets based on the molecular signature in breast cancer: genetic mutations and implications for current treatment paradigms.* Journal of hematology & oncology, 2019. **12**(1): p. 38.
10. Seijo, L.M., N. Peled, D. Ajona, M. Boeri, J.K. Field, G. Sozzi, R. Pio, J.J. Zulueta, A. Spira, and P.P. Massion, *Biomarkers in lung cancer screening: achievements, promises, and challenges.* Journal of Thoracic Oncology, 2019. **14**(3): p. 343-357.
11. Dhummakupt, E.S., G.M. Rizzo, M. Feasel, P.M. Mach, B.Q. Tran, D.O. Carmany, P.S. Demond, E.M. McBride, M. Maughan, and J.W. Sekowski, *Proteomic and Metabolomic Profiling Identify Plasma Biomarkers for Exposure to Ultra-low Levels of Carfentanil.* Toxicological Sciences, 2019. **167**(2): p. 524-535.
12. Cohen, L., A. Keegan, S.E. Melanson, and D.R. Walt, *Impact of clinical sample handling and processing on ultra-low level measurements of plasma cytokines.* Clinical biochemistry, 2019. **65**: p. 38-44.
13. Teng, J., L. Huang, L. Zhang, J. Li, H. Bai, Y. Li, S. Ding, Y. Zhang, and W. Cheng, *High-sensitive immunosensing of protein biomarker based on interfacial recognition-induced homogeneous exponential transcription.* Analytica chimica acta, 2019. **1067**: p. 107-114.
14. Macchia, E., L. Sarcina, R.A. Picca, K. Manoli, C. Di Franco, G. Scamarcio, and L. Torsi, *Ultra-low HIV-1 p24 detection limits with a bioelectronic sensor.* Analytical and bioanalytical chemistry, 2020. **412**(4): p. 811-818.
15. Burtis, C.A., E.R. Ashwood, and D.E. Bruns, *Tietz textbook of clinical chemistry and molecular diagnostics-e-book*. 2012: Elsevier Health Sciences.
16. McPherson, R.A., *Henry's Clinical Diagnosis and Management by Laboratory Methods: First South Asia Edition_e-Book*. 2017: Elsevier India.

17. Tabatabaei, M.S., R. Islam, and M. Ahmed, *Applications of gold nanoparticles in ELISA, PCR, and immuno-PCR assays: A review.* Analytica Chimica Acta, 2020.
18. Jeerapan, I., T. Sonsa-ard, and D. Nacapricha, *Applying Nanomaterials to Modern Biomedical Electrochemical Detection of Metabolites, Electrolytes, and Pathogens.* Chemosensors, 2020. **8**(3): p. 71.
19. Srivastava, M., N. Srivastava, P. Mishra, and B.D. Malhotra, *Prospects of Nanomaterials-enabled biosensors for COVID-19 detection.* Science of The Total Environment, 2020: p. 142363.
20. Shao, B. and Z. Xiao, *Recent achievements in exosomal biomarkers detection by nanomaterials-based optical biosensors-A review.* Analytica Chimica Acta, 2020.
21. Martin-Gracia, B., A. Martin-Barreiro, C. Cuestas-Ayllon, V. Grazu, A. Line, A. Llorente, J.M. de la Fuente, and M. Moros, *Nanoparticle-based biosensors for detection of extracellular vesicles in liquid biopsies.* Journal of Materials Chemistry B, 2020.
22. Singamaneni, S., M.C. LeMieux, H.P. Lang, C. Gerber, Y. Lam, S. Zauscher, P.G. Datskos, N.V. Lavrik, H. Jiang, and R.R. Naik, *Bimaterial microcantilevers as a hybrid sensing platform.* Advanced Materials, 2008. **20**(4): p. 653-680.
23. Nava Brezolin, A., J. Martinazzo, M.C. Blassioli-Moraes, A. Manzoli, J. Steffens, and C. Steffens, *Highly Sensitive Sensor for Trace Level Detection of Euschistus heros Pheromone.* Industrial Biotechnology, 2019. **15**(6): p. 357-364.
24. Sun, J., Y. Lu, L. He, J. Pang, F. Yang, and Y. Liu, *Colorimetric sensor array based on gold nanoparticles: Design principles and recent advances.* TrAC Trends in Analytical Chemistry, 2020. **122**: p. 115754.
25. El-Safty, S. and M. Shenashen, *Nanoscale dynamic chemical, biological sensor material designs for control monitoring and early detection of advanced diseases.* Materials Today Bio, 2020. **5**: p. 100044.
26. Sarihi, P., A.A. Shalmani, V. Araban, and M. Raoufi, *Nanoparticles for Biosensing*, in *Nanomaterials for Advanced Biological Applications*. 2019, Springer. p. 121-143.
27. Singh, P. and R. Yadava, *Nanosensors for health care*, in *Nanosensors for Smart Cities*. 2020, Elsevier. p. 433-450.
28. Rabbani, M., M.E. Hoque, and Z.B. Mahbub, *Nanosensors in biomedical and environmental applications: Perspectives and prospects*, in *Nanofabrication for Smart Nanosensor Applications*. 2020, Elsevier. p. 163-186.
29. Pal, K., *Nanofabrication for Smart Nanosensor Applications*. 2020: Elsevier.
30. Auría-Soro, C., T. Nesma, P. Juanes-Velasco, A. Landeira-Viñuela, H. Fidalgo-Gomez, V. Acebes-Fernandez, R. Gongora, M.J. Almendral Parra, R. Manzano-Roman, and M. Fuentes, *Interactions of nanoparticles and biosystems: microenvironment of nanoparticles and biomolecules in nanomedicine.* Nanomaterials, 2019. **9**(10): p. 1365.
31. Roy, A., O. Bulut, S. Some, A.K. Mandal, and M.D. Yilmaz, *Green synthesis of silver nanoparticles: biomolecule-nanoparticle organizations targeting antimicrobial activity.* RSC advances, 2019. **9**(5): p.

2673-2702.

32. Gonda, A., N. Zhao, J.V. Shah, H.R. Calvelli, H. Kantamneni, N.L. Francis, and V. Ganapathy, *Engineering Tumor-Targeting Nanoparticles as Vehicles for Precision Nanomedicine.* Med one, 2019. **4**.
33. Chen, W., X. Tian, W. He, J. Li, Y. Feng, and G. Pan, *Emerging functional materials based on chemically designed molecular recognition.* BMC Materials, 2020. **2**(1): p. 1-22.
34. Magro, M., A. Venerando, A. Macone, G. Canettieri, E. Agostinelli, and F. Vianello, *Nanotechnology-Based Strategies to Develop New Anticancer Therapies.* Biomolecules, 2020. **10**(5): p. 735.
35. Zeng, Y., S. Grandner, C.L. Oliveira, A.F. Thünemann, O. Paris, J.S. Pedersen, S.H. Klapp, and R. von Klitzing, *Effect of particle size and Debye length on order parameters of colloidal silica suspensions under confinement.* Soft Matter, 2011. **7**(22): p. 10899-10909.
36. Walker, S.A. and J.A. Zasadzinski, *Electrostatic control of spontaneous vesicle aggregation.* Langmuir, 1997. **13**(19): p. 5076-5081.
37. Chang, J., H. Pu, S.A. Wells, K. Shi, X. Guo, G. Zhou, X. Sui, R. Ren, S. Mao, and Y. Chen, *Semi-quantitative design of black phosphorous field-effect transistor sensors for heavy metal ion detection in aqueous media.* Molecular Systems Design & Engineering, 2019. **4**(3): p. 491-502.
38. Lu, Y., J.Y. Huang, C. Wang, S. Sun, and J. Lou, *Cold welding of ultrathin gold nanowires.* Nature nanotechnology, 2010. **5**(3): p. 218-224.
39. Selid, P.D., H. Xu, E.M. Collins, M. Striped Face-Collins, and J.X. Zhao, *Sensing mercury for biomedical and environmental monitoring.* Sensors, 2009. **9**(7): p. 5446-5459.
40. Choi, Y.-E., J.-W. Kwak, and J.W. Park, *Nanotechnology for early cancer detection.* Sensors, 2010. **10**(1): p. 428-455.
41. Mathew, R. and A.R. Sankar, *A review on surface stress-based miniaturized piezoresistive SU-8 polymeric cantilever sensors.* Nano-micro letters, 2018. **10**(2): p. 35.
42. Vashist, S.K. and J.H. Luong, *Microcantilever-Based Sensors*, in *Handbook of Immunoassay Technologies*. 2018, Elsevier. p. 305-332.
43. Haag, A.-L., *Potential-Driven Surface Stress of a Cantilever-Based Sensor*. 2016, Doctoral Dissertation. Montreal, Canada: McGill University.
44. Lah, N.A.C., M. Samykano, and S. Trigueros, *Nanoscale metal particles as nanocarriers in targeted drug delivery system.* Journal of Nanomedicine Research, 2016. **4**(2).
45. Lah, N.A.C. and S. Trigueros, *Synthesis and modelling of the mechanical properties of Ag, Au and Cu nanowires.* Science and technology of advanced materials, 2019. **20**(1): p. 225-261.
46. Azimzadeh, M., N. Nasirizadeh, M. Rahaie, and H. Naderi-Manesh, *Early detection of Alzheimer's disease using a biosensor based on electrochemically-reduced graphene oxide and gold nanowires for the quantification of serum microRNA-137.* RSC advances, 2017. **7**(88): p. 55709-55719.
47. Nodoushan, S.M., N. Nasirizadeh, R. Kachuei, and A.A.I. Fooladi, *Electrochemical detection of aflatoxin B1: an aptasensor prepared using graphene oxide and gold nanowires.* Analytical Methods,

2019. **11**(47): p. 6033-6042.

48. Letchumanan, I., S.C. Gopinath, M. Md Arshad, M.S. Mohamed Saheed, V. Perumal, C.H. Voon, and U. Hashim, *Gold-Nanohybrid Biosensors for Analyzing Blood Circulating Clinical Biomacromolecules: Current Trend toward Future Remote Digital Monitoring.* Critical Reviews in Analytical Chemistry, 2020: p. 1-16.
49. Takemura, K., J. Satoh, J. Boonyakida, S. Park, A.D. Chowdhury, and E.Y. Park, *Electrochemical Detection of White Spot Syndrome Virus With a Silicone Rubber Disposable Electrode Composed of Graphene Quantum Dots and Gold Nanoparticle-embedded Polyaniline Nanowires.* 2020.
50. Tian, Y., X. Li, F. Wang, C. Gu, Z. Zhao, H. Si, and T. Jiang, *SERS-based immunoassay and degradation of CA19-9 mediated by gold nanowires anchored magnetic–semiconductor nanocomposites.* Journal of Hazardous Materials, 2020: p. 124009.
51. Jahanmahin, O., D.J. Kirby, B.D. Smith, C.A. Albright, Z.A. Gobert, C.D. Keating, and K.A. Fichthorn, *Assembly of Gold Nanowires on Gold Nanostripe Arrays: Simulation and Experiment.* The Journal of Physical Chemistry C, 2020. **124**(17): p. 9559-9571.
52. Makvandi, P., C.y. Wang, E.N. Zare, A. Borzacchiello, L.n. Niu, and F.R. Tay, *Metal-based nanomaterials in biomedical applications: Antimicrobial activity and cytotoxicity aspects.* Advanced Functional Materials, 2020: p. 1910021.
53. De Mori, A., R.S. Jones, M. Cretella, G. Cerri, R.R. Draheim, E. Barbu, G. Tozzi, and M. Roldo, *Evaluation of antibacterial and cytotoxicity properties of silver nanowires and their composites with carbon nanotubes for biomedical applications.* International Journal of Molecular Sciences, 2020. **21**(7): p. 2303.
54. Ben Tahar, I., P. Fickers, A. Dziedzic, D. Płoch, B. Skóra, and M. Kus-Liśkiewicz, *Green pyomelanin-mediated synthesis of gold nanoparticles: modelling and design, physico-chemical and biological characteristics.* Microbial Cell Factories, 2019. **18**(1): p. 210.
55. Attarilar, S., J. Yang, M. Ebrahimi, Q. Wang, J. Liu, Y. Tang, and J. Yang, *The toxicity phenomenon and the related occurrence in metal and metal oxide nanoparticles: A brief review from the biomedical perspective.* Frontiers in Bioengineering and Biotechnology, 2020. **8**.
56. Kim, Y.-J., C.-J. Yoo, U. Lee, and Y.-M. Yoo, *Cytotoxicity of gold nanorods and nanowires on cultivated neural precursor cells.* Journal of nanoscience and nanotechnology, 2015. **15**(8): p. 5617-5623.
57. Li, X.-P., K.-Y. Qu, F. Zhang, H.-N. Jiang, N. Zhang, C. Nihad, C.-M. Liu, K.-H. Wu, X.-W. Wang, and N.-P. Huang, *High-aspect-ratio water-dispersed gold nanowires incorporated within gelatin methacrylate hydrogels for constructing cardiac tissues in vitro.* Journal of Materials Chemistry B, 2020. **8**(32): p. 7213-7224.
58. Xiao, T., J. Huang, D. Wang, T. Meng, and X. Yang, *Au and Au-Based nanomaterials: Synthesis and recent progress in electrochemical sensor applications.* Talanta, 2020. **206**: p. 120210.
59. Assis, P.A.d., S.B.d. Andrade, C.M.C.d. Oliveira, P.M.d. Araújo, S. Grangeiro Júnior, and S.V.V. Ramos, *Development and validation of a microbial counting method for mebendazole oral suspension.* Brazilian Journal of Pharmaceutical Sciences, 2011. **47**: p. 555-563.

60. Feng, H., Y. Yang, Y. You, G. Li, J. Guo, T. Yu, Z. Shen, T. Wu, and B. Xing, *Simple and rapid synthesis of ultrathin gold nanowires, their self-assembly and application in surface-enhanced Raman scattering.* Chemical Communications, 2009(15): p. 1984-1986.
61. de Moraes, D.A., J.B.S. Junior, F.F. Ferreira, V.V. Mogili, and L.C. Varanda, *Gold nanowires growth through stacking fault mechanism by oleylamine-mediated synthesis.* Nanoscale, 2020.
62. Fontes, E., J. Nandenha, R. De Souza, F. Antonio, P. Homem-de-Mello, and A. Neto, *Au core stabilizes CO adsorption onto Pd leading to CO2 production.* Materials Today Advances, 2020. **6**: p. 100070.
63. Kirichkov, M.V., A.A. Guda, A.P. Budnyk, A.L. Bugaev, T.A. Lastovina, V.V. Shapovalov, S.A. Guda, A.L. Trigub, Y.V. Rusalev, and A.V. Chernyshev, *X-ray and optical characterization of the intermediate products in the Au3+ reduction process by oleylamine.* Radiation Physics and Chemistry, 2018.
64. Liu, X., J. Kang, B. Liu, and J. Yang, *Separation of gold nanowires and nanoparticles through a facile process of centrifugation.* Separation and Purification Technology, 2018. **192**: p. 1-4.
65. Kim, J.-K., S.-A. Lee, S. Shin, J.-Y. Lee, K.-W. Jeong, Y.H. Nan, Y.S. Park, S.Y. Shin, and Y. Kim, *Structural flexibility and the positive charges are the key factors in bacterial cell selectivity and membrane penetration of peptoid-substituted analog of Piscidin 1.* Biochimica et Biophysica Acta (BBA) - Biomembranes, 2010. **1798**(10): p. 1913-1925.
66. Alves, C.S., M.N. Melo, H.G. Franquelim, R. Ferre, M. Planas, L. Feliu, E. Bardají, W. Kowalczyk, D. Andreu, and N.C. Santos, *Escherichia coli cell surface perturbation and disruption induced by antimicrobial peptides BP100 and pepR.* Journal of Biological Chemistry, 2010. **285**(36): p. 27536-27544.
67. Kwasnik, K., *Magnetic Resonance Force Microscopy Using Nanotubes and Nanowires*. 2004, Boston College. College of Arts and Sciences.
68. Nutting, J. and J. Nuttall, *The malleability of gold.* Gold Bulletin, 1977. **10**(1): p. 2-8.
69. Tremblay, C., G. Wheeler, and A. Oteri, *PhotonAssay™–Efficient & bulk gold analysis in the modern world.* ASEG Extended Abstracts, 2019. **2019**(1): p. 1-4.
70. Mirkin, C.A., *In My Element: Gold.* Chemistry–A European Journal, 2019. **25**(33): p. 7777-7778.
71. Lee, J.-H., S.U.S. Choi, S.P. Jang, and S.Y. Lee, *Production of aqueous spherical gold nanoparticles using conventional ultrasonic bath.* Nanoscale research letters, 2012. **7**(1): p. 420-420.
72. Beretta, S., M. Bosi, L. Seravalli, N. Musayeva, and C. Ferrari, *Orientation of germanium nanowires on germanium and silicon substrates for nanodevices.* Materials Today: Proceedings, 2020. **20**: p. 30-36.
73. Zhang, Y. and H. Liu, *Nanowires for High-Efficiency, Low-Cost Solar Photovoltaics.* Crystals, 2019. **9**(2): p. 87.
74. Zhang, K., X. Li, W. Dai, F. Toor, and J.P. Prineas, *Carrier Recombination in the Base, Interior, and Surface of InAs/InAlAs Core–Shell Nanowires Grown on Silicon.* Nano Letters, 2019. **19**(7): p. 4272-4278.

75. FrozandehMehr, E., A. Tarlani, and S. Farhadi, *Cetyltrimethylammonium bromide (CTAB) bloated micelles and merged CTAB/bolaamphiphiles self-assembled vesicles toward the generation of highly porous alumina as efficacious inorganic adsorbents.* Langmuir, 2019. **35**(34): p. 11188-11199.
76. Llombart, P., M.A. Palafox, L.G. MacDowell, and E.G. Noya, *Structural transitions and bilayer formation of CTAB aggregates.* Colloids and Surfaces A: Physicochemical and Engineering Aspects, 2019. **580**: p. 123730.
77. Zorawar, S. and I. Singh, *CTAB Surfactant Assisted and High pH Nano-Formulations of CuO Nanoparticles Pose Greater Cytotoxic and Genotoxic Effects.* Scientific Reports (Nature Publisher Group), 2019. **9**(1).
78. FrozandehMehr, E., A. Tarlani, and S. Farhadi, *CTAB bloated micelles and merged CTAB/bolaamphiphiles self-assembled vesicles toward the generation of highly porous alumina as efficacious inorganic adsorbents.*
79. Vlachy, N., M. Drechsler, D. Touraud, and W. Kunz, *Anion specificity influencing morphology in catanionic surfactant mixtures with an excess of cationic surfactant.* Comptes Rendus Chimie, 2009. **12**(1-2): p. 30-37.
80. Zhi, D., S. Zhang, S. Cui, Y. Zhao, Y. Wang, and D. Zhao, *The headgroup evolution of cationic lipids for gene delivery.* Bioconjugate chemistry, 2013. **24**(4): p. 487-519.
81. Kumar, S., H. Patel, and S.R. Patil, *Test of Hofmeister-like series of anionic headgroups: clouding and micellar growth.* Colloid and Polymer Science, 2013. **291**(9): p. 2069-2077.
82. Rahimi-Nasrabadi, M., A. Ghaderi, H.R. Banafshe, M. Eghbali-Arani, M. Akbari, F. Ahmadi, S. Pourmasoud, and A. Sobhani-Nasab, *Preparation of Co 2 TiO 4/CoTiO 3/Polyaniline ternary nano-hybrids for enhanced destruction of agriculture poison and organic dyes under visible-light irradiation.* Journal of Materials Science: Materials in Electronics, 2019. **30**(17): p. 15854-15868.
83. Enea, M., M. Peixoto de Almeida, P. Eaton, D. Dias da Silva, E. Pereira, M.E. Soares, M.d.L. Bastos, and H. Carmo, *A multiparametric study of gold nanoparticles cytotoxicity, internalization and permeability using an in vitro model of blood–brain barrier. Influence of size, shape and capping agent.* Nanotoxicology, 2019. **13**(7): p. 990-1004.
84. Duan, H., D. Wang, and Y. Li, *Green chemistry for nanoparticle synthesis.* Chemical Society Reviews, 2015. **44**(16): p. 5778-5792.
85. Buchman, J.T., N.V. Hudson-Smith, K.M. Landy, and C.L. Haynes, *Understanding nanoparticle toxicity mechanisms to inform redesign strategies to reduce environmental impact.* Accounts of chemical research, 2019. **52**(6): p. 1632-1642.
86. Shebl, R.I., F. Farouk, and H.M.E.-S. Azzazy, *Effect of Surface Charge and Hydrophobicity Modulation on the Antibacterial and Antibiofilm Potential of Magnetic Iron Nanoparticles.* Journal of Nanomaterials, 2017. **2017**: p. 3528295.
87. Calabrese, V., M.A. da Silva, J. Schmitt, K.M.Z. Hossain, J.L. Scott, and K.J. Edler, *Charge-driven interfacial gelation of cellulose nanofibrils across the water/oil interface.* Soft Matter, 2020. **16**(2): p. 357-365.

88. Silva, A.M., C. Martins-Gomes, T.E. Coutinho, J.F. Fangueiro, E. Sanchez-Lopez, T.N. Pashirova, T. Andreani, and E.B. Souto, *Soft cationic nanoparticles for drug delivery: Production and cytotoxicity of solid lipid nanoparticles (SLNs).* Applied Sciences, 2019. **9**(20): p. 4438.
89. Salajkova, S., M. Sramek, D. Malinak, F. Havel, K. Musilek, M. Benkova, O. Soukup, P. Vasicova, L. Prchal, and R. Dolezal, *Highly hydrophilic cationic gold nanorods stabilized by novel quaternary ammonium surfactant with negligible cytotoxicity.* Journal of Biophotonics, 2019. **12**(12): p. e201900024.
90. Ramanaiah, M., P. Seetharam, M. Balakrishna, and B.R. Raju, *Potentiometric studies of complex equlibria of CaII, MgII and ZnII with 5-sulphosalicylic acid in cationic micelles of CTAB.* Heliyon, 2019. **5**(8): p. e02157.
91. Wang, L., X. Jiang, Y. Ji, R. Bai, Y. Zhao, X. Wu, and C. Chen, *Surface chemistry of gold nanorods: origin of cell membrane damage and cytotoxicity.* Nanoscale, 2013. **5**(18): p. 8384-91.
92. Beurton, J., P. Lavalle, A. Pallotta, T. Chaigneau, I. Clarot, and A. Boudier, *Design of surface ligands for blood compatible gold nanoparticles: effect of charge and binding energy.* International Journal of Pharmaceutics, 2020: p. 119244.

Figures

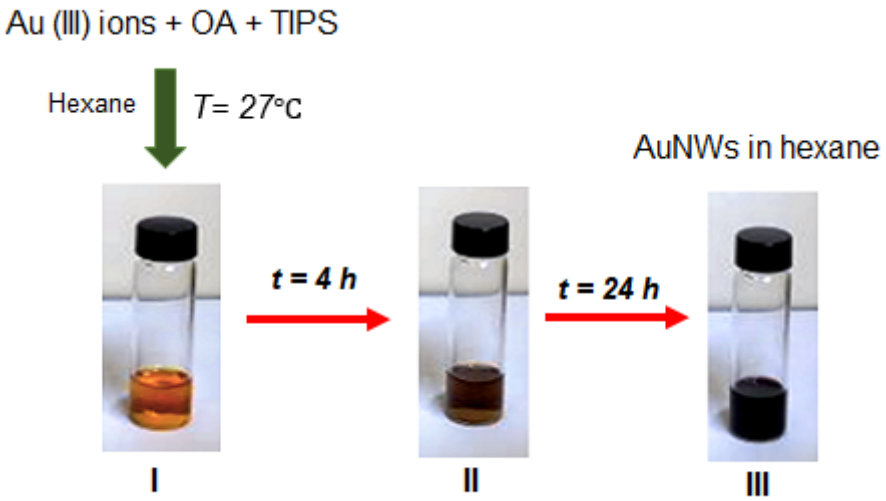

Figure 1

As-synthesised AuNWs reaction formation flow. (I) The solution of HAuCl4.3H2O + OA +TIPS after 1 minute of the mixture. (II) After the mixture is left at room temperature for 4 h and (III) 24 h. The reaction product has a dark violet colour solution after 24 h.

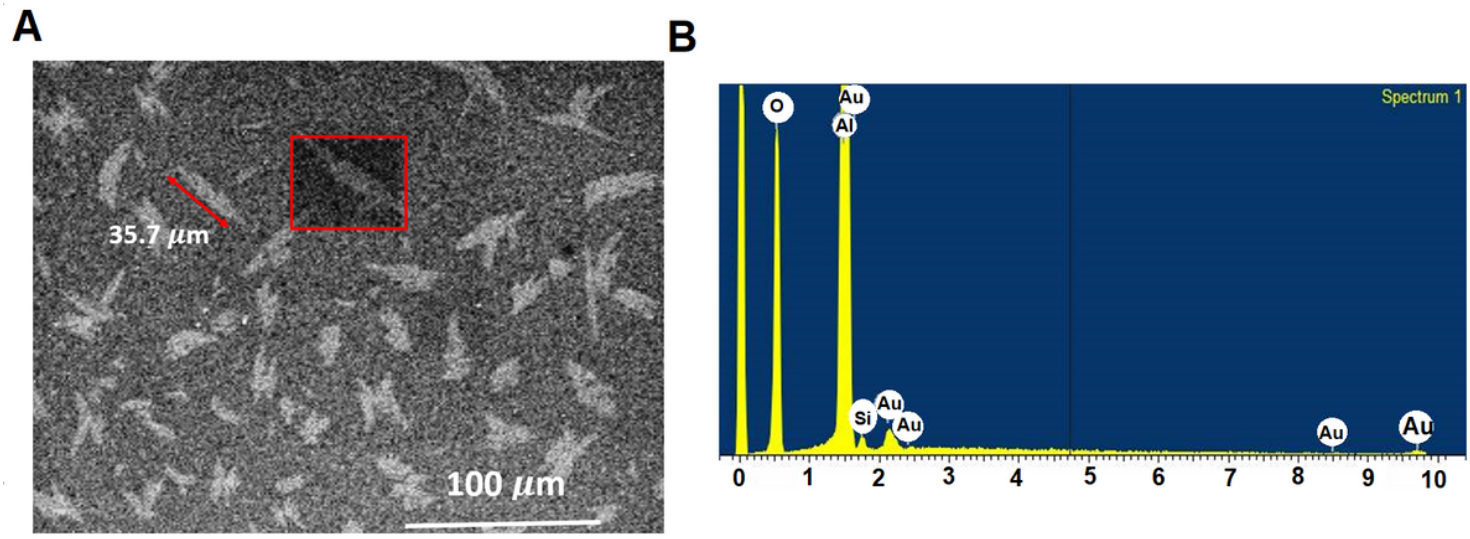

Figure 2

A. The representative FESEM micrograph of the as-synthesised AuNWs. The enlarged figure (yellow rectangular) reveals the parallel self-assembly arrangement of close-packed AuNWs bundles. The small parallel bundle highlighted in yellow circle showed that the bundle of the nanowires has a diameter size of ~200 nm. Noted that the individual AuNWs in each bundle would possess the arrangement and the individual AuNWs size that are almost similar to the original method reported by Feng et al., (Figure with asterisk mark is reproduced from ref. [60] with permission from The Royal Society of Chemistry). B. The EDX spectrum analysis of the as-synthesised AuNWs recorded for the selected area of AuNWs (red rectangle) taken from image A.

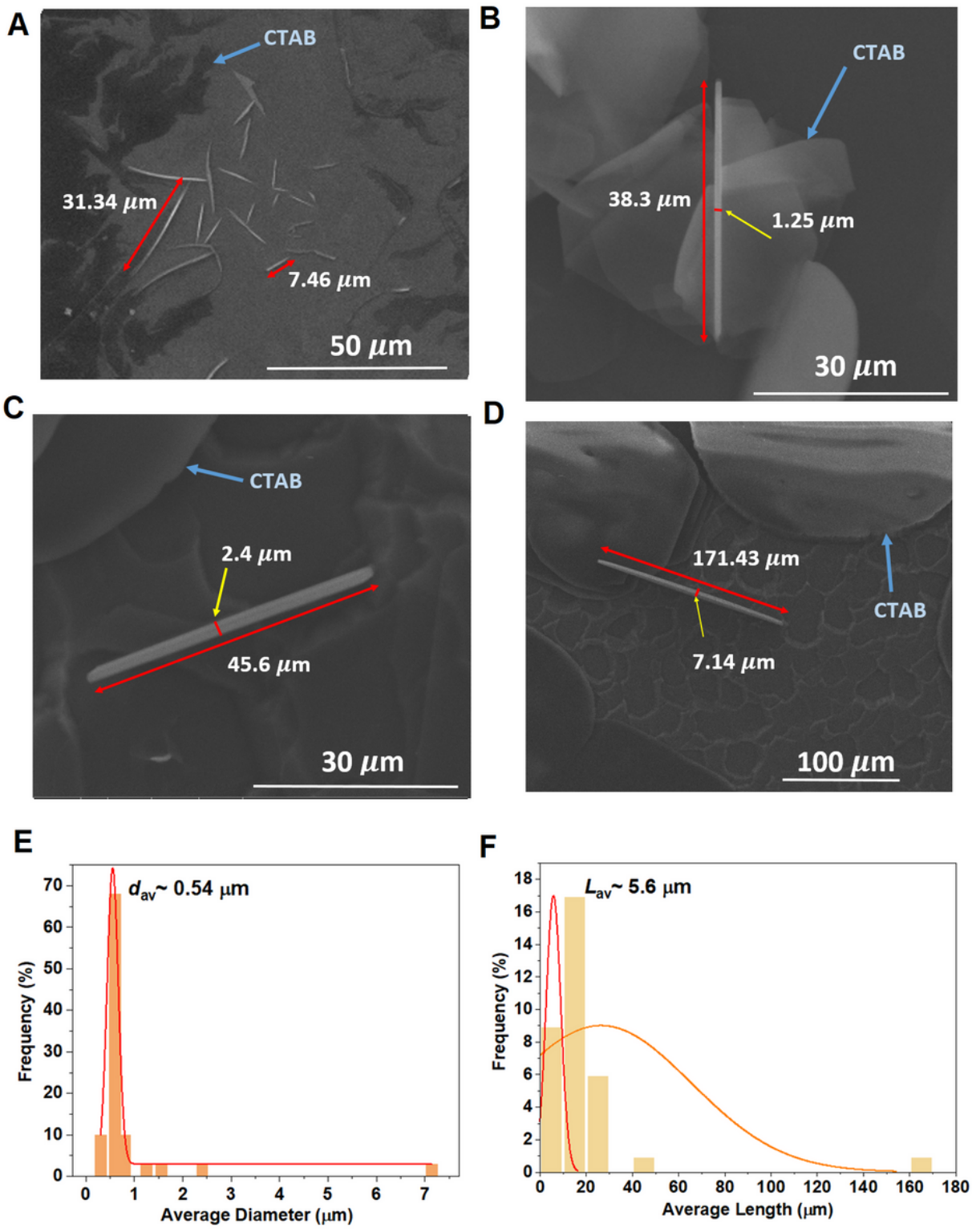

Figure 3

A. Representative of FESEM images of sonicated commercial AuNWs with CTAB as a capping agent. B, C and D indicate the individual AuNWs. E. The corresponding diameter and F. length distributions of the commercial AuNWs in an aqueous solution of CTAB. The average diameter and length of the AuNWs are 0.54 and 5.6 μm, respectively, indicated by the Gaussian plot (red line).

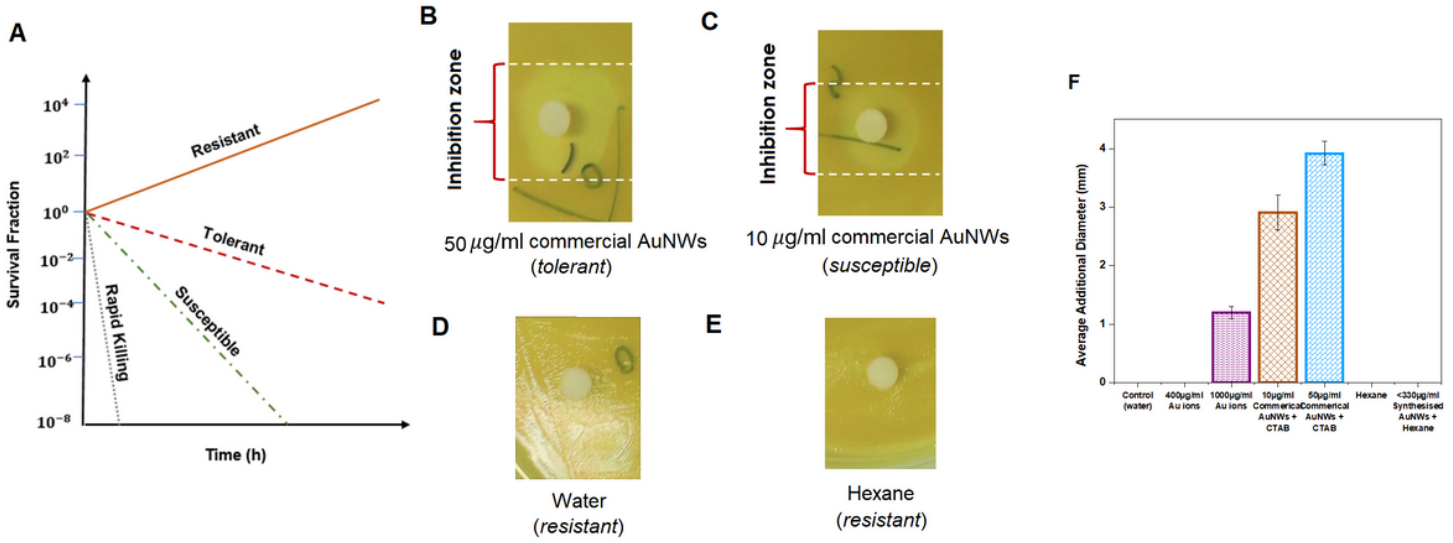

Figure 4

The representative image of E.coli DH5α responses to the AuNWs solutions. The disc diffusion assay results with E.coli DH5α cells (100 µl) on LB agar overlay. A and B indicate the white dotted lines mark the diameter of the white zone where the growth of E.coli DH5α is prevented by the AuNWs (inhibition area). A is a tolerant strain with B is the susceptible strain. A slightly larger zone of inhibition is seen for tolerant strain due to growth delayed. C and D are referring to control sample of water and hexane solutions, respectively. Both show resistant strain. E. Schematic illustration on the differences between the fraction of surviving bacteria for resistant, tolerant, susceptible and rapid killing strains. F. Disc diffusion measurements obtained using several concentrations of Au ions and both the as-synthesised and commercial AuNWs. The bars represent one standard error.

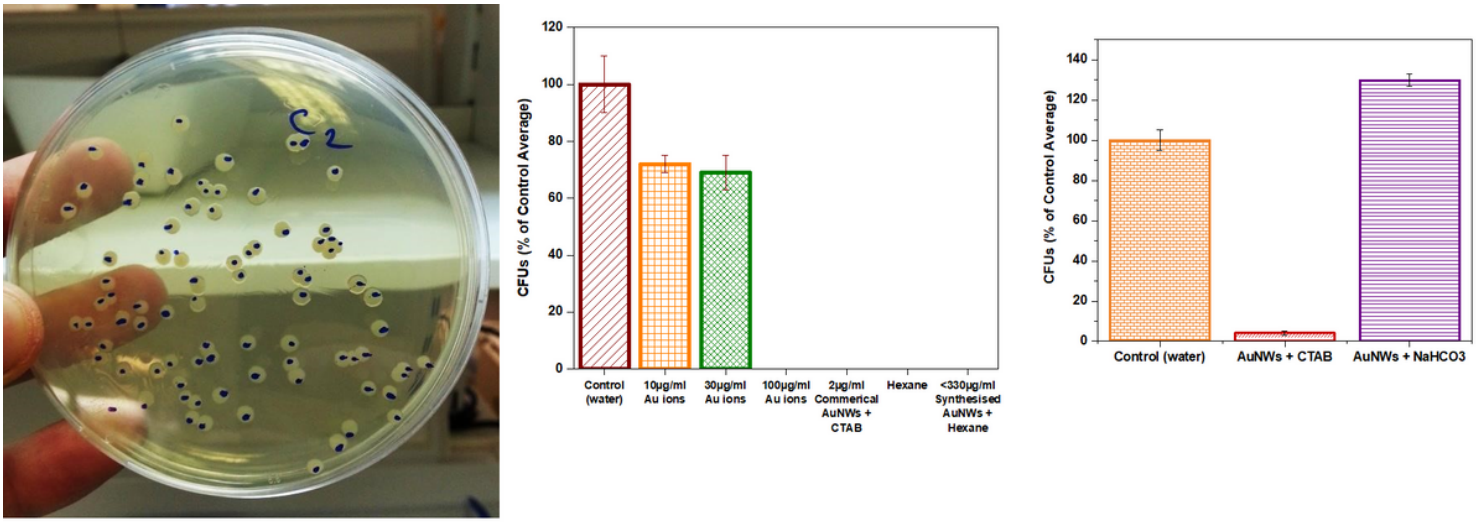

Figure 5

A. The representative of AuNWs antimicrobial CFU enumeration based on the individual colonies of E.coli DH5α formed after 24 hours. Blue marker was used to mark the colonies with dots marking at the bottom side of the petri dish. B. The number of bacterial colonies (%) appeared in agar plated treated with control (water), 10, 30 µg/ml and 100 µg/ml of Au ions, 2 µg/ml of commercial AuNWs suspended in CTAB, hexane and < 330µg/ml as-synthesised AuNWs in hexane. C. Activity of antimicrobial CFU assay of AuNWs capped with CTAB and $NaHCO_3$ after 24 hours of plate-incubation. Water is used as a control sample.

Supplementary Files

This is a list of supplementary files associated with this preprint. Click to download.

- SupplementaryMaterialsMICFD2000239.docx